Magnetic Properties of MnS

Antiferromagnetic Long Range Order and Hysteresis

P.S.P. Steger[1] and V. Yu. Pomjakushin[2,⋆]

[1] Swiss Federal Institute of Technology, CH-8092 Zurich, Switzerland
e-mail: psteger@phys.ethz.ch
[2] Laboratory for Neutron Scattering, ETH Zurich and Paul Scherrer Institut, CH-5232 Villigen PSI, Switzerland

Draft version August 24, 2008

ABSTRACT

Aims. We wanted to reproduce the results of a measurement done by Shull 1951, where he studied the lattice structure of MnO and its long range order antiferromagnetism. We investigated a slightly different sample, MnS.
Methods. We analyzed a polycrystalline sample of MnS at HRPT, a high-resolution powder diffractometer at the spallation neutron source SINQ, PSI.
Results. MnS belongs to the crystallographic space group $Fm\bar{3}m$ with $a = 5.209$Å the lattice constant of the elementary nuclear cell. It shows antiferromagnetic long range order below a Néel temperature of 150 K with layers of magnetically ordered Mn atoms along several directions. The temperature dependence of the relative strength between nuclear and magnetic peaks is given by a linear decay. We have detected an unexpected hysteresis behaviour of our sample: the Néel temperature depends on whether it is approached from lower or higher temperatures. The peaks from the antiferromagnetic structure built up at 150 K, when the sample was cooled down from room temperature, but did not vanish below 180 K, if it was heated.

Key words. Antiferromagnetism – Hysteresis – HRPT

1. Introduction

Magnetic scattering effects are introduced in detail in the books of (Ash, 1976), (Bac, 1975) and (Squ, 1978). We will give a short summary of basic concepts and definitions in section 2. The characteristics of HRPT are outlined in section 3. Our results for nuclear and antiferromagnetic structure are presented in sections 4.1 and 4.2, respectively. We show how the intensity of the magnetic reflexes depend on temperature in 4.3, followed by a discussion on the hysteresis effect in section 4.4. Finally, the summary in 5 concludes with a preview on possible follow-up measurements.

2. Crystallographic structure

In order to determine the nuclear structure of a crystal, one determines the diffraction pattern of thermal neutrons. The crystal should show paramagnetic behavior, such that no additional contributions to the diffraction pattern from magnetic structures occur. This condition is most suitably ensured by heating the sample to a temperature well above the Néel temperature T_N; MnS with a tabulated $T_N = 151$K is paramagnetic at room temperature. The positions of the reflexes in the diffraction pattern are calculated using Bragg's diffraction formula:

$$2d \sin\theta = \lambda, \tag{1}$$

where

$$d = d_{hk\ell} = \frac{a}{\sqrt{h^2 + k^2 + \ell^2}} \tag{2}$$

is the distance between two $(hk\ell)$-planes in reciprocal space. The additional suppression of several peaks due to destructive interference was taken into account by using the structure factor

$$S_{hk\ell} = [1 + (-1)^{h+k} + (-1)^{h+\ell} + (-1)^{k+\ell}] \sum_j b_j e^{i\boldsymbol{Q}\cdot\boldsymbol{r}_j}, \tag{3}$$

derived for the two Mn and S ions in a sc lattice cube at positions $\boldsymbol{r}_j$ with atomar scattering lengths $b_{\mathrm{Mn}} = -3.73 \cdot 10^{-13}$cm and $b_{\mathrm{S}} = 2.847 \cdot 10^{-13}$cm. $\boldsymbol{Q}$ denotes the diffraction vector, which must equal a reciprocal vector $\boldsymbol{g}_{hk\ell} = h\boldsymbol{g}_1 + k\boldsymbol{g}_2 + \ell\boldsymbol{g}_3$ in order to satisfy Bragg's formula. Note that $S_{hk\ell} \neq 0$ only as long as the three Miller indices fulfill $h + k, k + \ell, h + \ell \in 2\mathbb{N}$. Otherwise the prefactor in eq. 3 vanishes.

3. Methods

The main concepts of HRPT are explained in (P. Fischer et al., 2000). It is based on a linear position-sensitive ^{3}He detector with 1600 wires permitting a resolution of 0.1°. Neutrons from a D_2O scatterer close to the SINQ target pass several filters and a monochromator before entering HRPT with a wavelength $\lambda = 1.8857$. Signals from the sample environment are suppressed to a high degree by use of a radial collimator.
We verified that the detector worked properly using a cylindrical standard sample out of $Na_2Ca_3Al_2F_{14}$, looking at the given wavelength and identifying characteristic peaks, cf. fig. 1. No extraordinary patterns were found. As a quantity used in connection with absorption coefficients, the linear absorption coefficient was measured to be

$$\mu r = -\frac{\ln(I/I_0)}{2} = 0.168 \pm 0.001 \tag{4}$$

⋆ Advisor and technical assistance

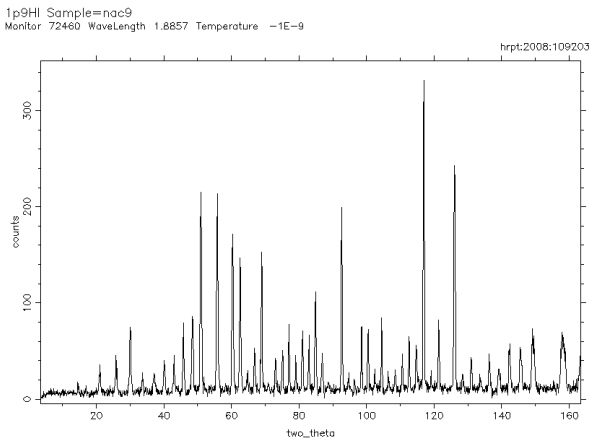

Fig. 1. Standard sample $Na_2Ca_3Al_2F_{14}$ at $\lambda = 1.8857$Å.

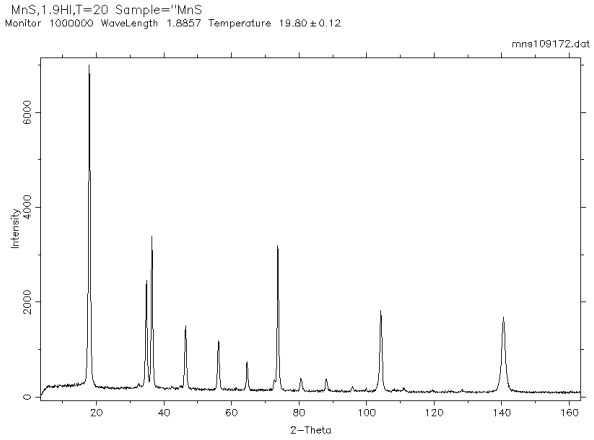

Fig. 2. Nuclear and antimagnetic peaks in the diffraction pattern from MnS at 20K.

with direct beam intensity I_0 and attenuated intensity I, after the sample was held into the direct beam.

4. Results

4.1. Pattern of Nuclear Peaks

In the range $0^o < 2\theta < 160^o$, we found four peaks at room temperature, in good agreement with the lowest diffraction peaks predicted from a NaCl-type structure, cf. table 5. We determined the lattice constants from the nuclear diffraction peaks at 20K with a mean value of $a_{\text{exp}} = 5.209 \pm 0.003$Å, which is 2‰ higher than the literature value of $a_{\text{th}} = 5.199$Å at 0K. In the table, the predicted values used the mean value of the experimental results rather than the theoretical one.

$(hk\ell)$	predicted	measured	difference
(111)	36.5706^o	36.4754^o	2.6‰
(311)	73.8521^o	73.7978^o	0.1‰
(331)	104.2934^o	104.2681^o	0.2‰
(333),(511)	140.5242^o	140.5490^o	0.2‰

(5)

The direct beam at 0^o which includes also simple forward scattering was not recorded. Peaks corresponding to scattering off (200), (220) or higer, all-even planes are suppressed by the structure factor by a factor of at least 50 with relation to the all-odd ones. – The intensities of the four peaks were determined both experimentally and using

$$I(Q) = C \cdot A(Q) \cdot \frac{\lambda^3}{\sin\theta \sin 2\theta} \cdot N \frac{(2\pi)^3}{v_0} F^2(Q) \cdot M_{hk\ell} \tag{6}$$

with scale factor C, absorption $A(Q)$, slowly changing with Q; wavelength λ of the incoming wave, scattering angle θ, number of cells N, volume per cell v_0, structure factor $F(Q)$ and multiplicity $M_{hk\ell}$. The multiplicity arises from the fact that each Miller index could also be flipped to the conjugated value, for instance (111) = $(\bar{1}11)$. It is therefore given by

$$M_{hk\ell} = 2^3 \cdot \frac{3!}{(\delta_{hk} + \delta_{k\ell} + 1)!}, \tag{7}$$

provided that the indices are ordered by their absolute values and $h, k, \ell \neq 0$. The relation of the experimentally integrated intensities was approximately given by 4 : 4 : 2 : 4 – compared to the predicted 4.00 : 3.89 : 2.93 : 3.73 – while their maximum values given by the resolution function showed a relation 2:2:1:1. See the next section for the respective equations.
One could see that there was a rising background towards lower scattering angles. The intensity under this background equals roughly the intensity of the magnetic peaks that were observed at lower temperatures.

4.2. Pattern of Magnetic Peaks

(C.G. Shull et al., 1951) find that MnO shows antiferromagnetic behavior over long range order. Ferromagnetic planes along (111) are stacked with layers of antiparallel magnetic orientation. The magnetic elementary cell has therefore twice the lattice constant as the nuclear one. This structure was verified with MnO and implicitly postulated for MnS, which only has an O atom replaced by the chemically similar S and should therefore build the same structure.
Below 150K, a series of additional single peaks developed at moderately low scattering angles for our sample, cf. fig. 2. These correspond to the scattering off an additional antiferromagnetic structure in the material. At low temperatures of 19.80K, the background stated above could not be distinguished within the statistical errors below 20^o.
A total of eight additional peaks was fitted to the model of antiferromagnetic layers in MnS; table 8 shows the quality of the predictions. $a = 5.211$Å was determined in the same way as was used for the nuclear peaks, but this time using only the magnetic peaks. If all peaks available are taken into account, the mean changes a little towards $a = 5.210$Å.

$(hk\ell)$	predicted	measured	error
(1/2,1/2,1/2)	18.0292^o	17.9457^o	5‰
(3/2,1/2,1/2)	34.9189^o	34.8330^o	3‰
(3/2,3/2,1/2)	46.4469^o	46.4429^o	2‰
(5/2,1/2,1/2)	56.0761^o	56.1562^o	1‰
(5/2,3/2,1/2)	64.7129^o	64.6731^o	2‰
(5/2,3/2,3/2)	72.7694^o	72.80^o	5‰
(5/2,5/2,1/2)	80.4864^o	81.1^o	6‰
(5/2,5/2,3/2)	88.0317^o	88.0^o	6‰

(8)

The errors in the last row increase with decreasing intensity, mostly because the exact peak was smeared out into the Voigt

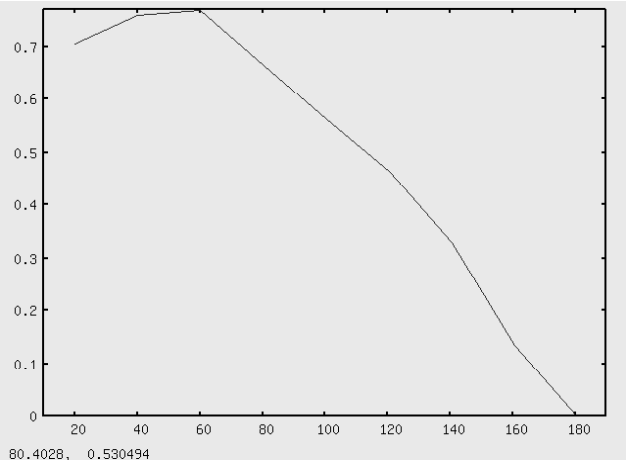

Fig. 3. Relative integrated intensity $\xi(T)$ for the peaks (3/2,1/2,1/2), (111), as function of temperature (in K).

wings at lower intensities. The intesity itself drops faster than $(2\theta)^{-1}$, which agrees with theory, predicting

$$I(Q) \propto N\frac{(2\pi)^3}{v_0}\cdot F_{m\perp}^2(Q)\cdot M_{hk\ell}, \tag{9}$$

$$F(Q) \propto \sum_j f_j(Q)e^{i\boldsymbol{Q}\cdot\boldsymbol{r}_j}\cdot\boldsymbol{\mu}_\perp, \tag{10}$$

$$\boldsymbol{\mu}_\perp = \boldsymbol{\mu} - \frac{\boldsymbol{Q}(\boldsymbol{\mu}\cdot\boldsymbol{Q})}{Q^2}. \tag{11}$$

The ratio of the magnetic $(1/2,1/2,1/2)$ and the nuclear (111) peak intensities integrated over all 2θ could be determined using the experimentally found $2\theta = 17.9457^{\text{o}}, 36.4754^{\text{o}}$ and

$$I_{\text{nuc,mag}} \propto \frac{1}{\sin\theta\sin 2\theta}F_{\text{nuc,mag}}^2\cdot M_{hk\ell,\text{nuc,mag}} \tag{12}$$

as well as

$$\mu = \sqrt{\frac{I_m}{I_n}}\sqrt{\frac{M_n\cdot L_n}{M_m L_m}}\cdot\frac{F_n}{F'_m} \tag{13}$$

with multiplicities M_m, M_n, Lorentz factors L_n, L_m and the magnetic stream factor $F'_m = F_m/\mu$ to have a mean value of

$$\mu = 4.17\mu_B \tag{14}$$

4.3. Temperature dependence

The integrated experimental intensities for the second antiferromagnetic and the nearby nuclear peak,

$$\xi(T) = \frac{\int_{2\theta-\varepsilon}^{2\theta+\varepsilon} d(2\theta)\, I_{(3/2,1/2,1/2)}(T,2\theta)}{\int_{2\theta-\varepsilon}^{2\theta+\varepsilon} d(2\theta)\, I_{(111)}(T,2\theta)}, \tag{15}$$

are plotted in fig. 3 as function of sample temperature T. Those two peaks can be conveniently compared in intensity, since they have similar scale and absorption factors, even the Lorentz factor $\lambda^3/\sin\theta\sin 2\theta$ does not differ more than 10%. We see an almost linear decrease with a slope of $-6\cdot 10^{-3}$/K starting at around 60 K. $\xi(T)$ is directly proportional to the ordered magnetic moment $\mu(T)$ of the Mn ions, as it represents a measure of the mean magnetic order normalized to the nuclear contributions. This was used already in section 4.2.

4.4. Hysteresis of MnO

The plot in fig. 3 was determined by heating the sample from 20K up to room temperature. At the tabulated Néel temperature of 150K, there still existed a considerable amount of magnetic order. This was not observed previously when the sample was cooled down from room temperature, a hint to hysteresis. The slow heat transport at such low temperatures and the poor thermal coupling due to a vacuum surrounding the sample were taken into account; the measurement series was carried out again with smaller temperature steps and longer acclimating times between individual measurements; the antiferromagnetic peak did not lose much intensity.

5. Summary

We have determined the nuclear structure of MnS as simple cubic with lattice constant $a = 5.209 \pm 0.003$Å. Antiferromagnetic long range order could be seen at temperatures below 150K after cooling, and up to 180K after heating. This hints to an additional hysteretic effect which was not expected. The NaCl-type lattice gives very good estimates for the positions of Bragg reflexes, both for nuclear and magnetic peaks, as long as the lattice constant is doubled. This is what was suspected from the measurements of Shull on MnO. The magnetic moment of the Mn ions follows a nearly linear decay starting at 60K.
In future experiments one should use a different sample of MnS to check whether the hysteresis could be reproduced, as we were only able to scrutinize one sample. A better thermal coupling to a cryostat would be preferable as well.

References

Solid State Physics (Saunders College Publishing, 1976).
Neutron Diffraction (Clarendon Press Oxford, 1975).
Introduction to the Theory of Thermal Neutron Scattering (Cambridge University Press, 1978).
P. Fischer, G. Frey, M. Koch, M. Könnecke, V. Pomjakushin, J. Schefer, R. Thut, N. Schlumpf, R. Bürge, U. Greuter, et al., *High-resolution powder diffractometer HRPT for thermal neutrons at SINQ*, Physica B **276–278**, 146 (2000).
C.G. Shull, W.A. Strauser, and E.O. Wollan, *Neutron Diffraction by Paramagnetic and Antiferromagnetic Substances*, Physical Review **83**, 333 (1951).